https://dx.doi.org/10.1016/j.istruc.2025.108356

Effectiveness and robustness of using nonlinear pendulum tuned mass damper inerters for wind-induced vibration mitigation of high-rise buildings

Xunchen Yang[a], Ruisheng Ma[a,b]*, Kaiming Bi[c,d]*, Huan Li[a], Xiuli Du[a]

[a] State Key Laboratory of Bridge Engineering Safety and Resilience, Beijing University of Technology, Beijing, China

[b] State Key Laboratory of Coastal and Offshore Engineering, Dalian University of Technology, Dalian, China

[c] Research Centre for Urban Hazards Mitigation (RCUHM), The Hong Kong Polytechnic University, Hong Kong, China

[d] Department of Civil and Environmental Engineering, The Hong Kong Polytechnic University, Hong Kong, China

Abstract: Tall buildings are at risk of experiencing vibrations induced by the wind because of their long fundamental periods and low inherent damping. These excessive vibrations can threaten the structural safety and the comfort of residents. For this reason, pendulum tuned mass dampers (PTMDs) are commonly employed to reduce the adverse vibrations of high-rise buildings. However, their applications are often accompanied by concerns over the large auxiliary mass required and overabundant swing angles. To tackle the above issues, this study investigates the potential of using inerters to enhance the conventional PTMDs for achieving more effective wind-induced vibration mitigation performance of high-rise buildings. In particular, the concepts and working mechanisms of two nonlinear pendulum tuned mass damper inerters (NPTMDIs) with different configurations are first presented. Subsequently, the analytical models of a high-rise building equipped with NPTMDIs are established, and the optimal parameters of NPTMDIs are obtained via genetic algorithm by minimizing the maximum top-floor absolute acceleration of the building structure. Ultimately, the vibration control effectiveness of the two NPTMDIs is evaluated and contrasted with that of a conventional PTMD. Moreover, the robustness of NPTMDIs against structure and device parameter variations is also comprehensively evaluated. The results demonstrate that NPTMDIs demonstrate greater effectiveness compared to PTMD in mitigating the wind-induced responses of the high-rise building with much smaller swing angles of the tip mass, and they exhibit better robustness against the mistuning issue induced by the perturbations of structural stiffness and damping. Besides, compared to NPTMDI with configuration II, the vibration control effectiveness and robustness of NPTMDI I are more significant.

Keywords: Nonlinear pendulum tuned mass damper inerters, clutched inerter, high-rise building,

optimization design, control effectiveness, wind-induced response, robustness

1. Introduction

The escalating cost of land in densely populated metropolitan areas is driving the development of slender high-rise buildings designed to maximize land use and optimize interior space efficiency. These structures, characterized by their slenderness and considerable height, are ideal solutions to the challenges posed by urbanization. However, these features that make them desirable also cause them to be vulnerable to external forces, particularly wind loads. Owing to their long fundamental periods and low inherent damping, slender tall buildings are highly vulnerable to vibrations induced by wind, which could substantially affect their serviceability performance, e.g., occupant comfort [1, 2]. A notable example occurred in 2021 when the 356 m Shenzhen SEG Plaza experienced significant swaying under moderate wind conditions, prompting widespread panic among building occupants and people in the surrounding area. Consequently, it is a key issue to effectively alleviate the wind-induced responses of high-rise buildings to acceptable thresholds.

Currently, three approaches are generally utilized to control excessive wind-induced vibrations of high-rise buildings, including (1) modifying properties of structures, e.g., stiffness and mass; (2) optimizing buildings' aerodynamic design; and (3) implementing supplementary passive or active vibration control devices that dissipate the vibration energy, namely structural vibration control [3]. Among these approaches, structural vibration control has gained widespread adoption in the realm of civil engineering owing to its exceptional performance and versatility in both existing and new structures [4]. The pendulum tuned mass damper (PTMD) is among the most frequently utilized devices for high-rise buildings, featuring a simple design that typically includes a pendulum rod and a tip mass [5, 6]. When a tall building oscillates under wind loads, the tip mass of PTMD can swing in the opposite direction of the building's motion, hence generating a counteracting force to help suppress vibrations. Sacks and Swallow [7] detailed the design and applications of PTMD for dynamic response mitigation of two tower structures exposed to wind loads. Tuan and Shang [8] implemented a PTMD system to the Taipei 101 Tower and numerically evaluated the dynamic responses of the building under both wind and earthquake loads. Meanwhile, Lu and Chen [9, 10] investigated the control effectiveness of using PTMD to mitigate the wind-induced vibrations of Shanghai Centre Tower. Matta [11] implemented a bidirectional PTMD onto a 42-storey high-rise building and numerically verified its vibration mitigation effectiveness. Wang et al. [12-14] developed

a PTMD with variable pendulum length (dubbed SAVP-TMD) and carried out experimental and numerical studies to assess its performance. The results showed that the SAVP-TMD could achieve superior control performance compared to the conventional PTMD by automatically re-tuning to the basic frequency of the structure. Additionally, Miguel et al. [15] employed multiple PTMDs to reduce the dynamic responses of a tall steel structure under wind loads. Although the existing PTMDs could effectively reduce structural vibration responses to some extent, they have not yet been extensively implemented in practical engineering applications due to the following concerns: (1) the effectiveness of a PTMD largely depends on its mass ratio, i.e., the ratio between the mass of its tip mass and the main structure. Generally, a large mass ratio is beneficial for attaining desirable control effectiveness. However, increasing the mass ratio not only adds to the structural load and thereby increases construction costs, but also complicates the connection system [16]; (2) under extreme loads (e.g., strong winds, waves, and earthquakes), the tip mass in PTMD may collide with the internal walls of structures, which can cause local damage or even structural failure, thus compromising structural safety; (3) PTMDs are sensitive to changes in the fundamental frequency of the controlled structure, a challenge known as the mistuning issue [17].

In the past few decades, the emergence of a novel two-terminal element known as 'inerter' coined by Smith [18] has offered a promising solution for overcoming the inherent limitations of traditional control devices. Essentially, an inerter can produce a force that correlates with the relative acceleration between its two terminals, distinguished by two attractive properties, namely mass amplification and negative stiffness effects [19]. Owing to these properties, various efficient inerter-based control devices [20] have been put forward and extensively investigated, e.g., tuned mass damper inerters (TMDIs) [21], negative stiffness inerter damper (NSID) [22], tuned viscous mass dampers (TVMDs) [23], inertial eddy current damper (IECD) [24], tuned inerter dampers (TIDs) [25], clutched inerter dampers (CIDs) [26, 27], rotational inertia damper (RID) [28], and tuned parallel inerter mass system (TPIMS) [29]. These inerter-based vibration control devices have been widely applied across various fields, including earthquake and wind engineering, and demonstrated superior vibration control performances. Researchers have extensively explored the performances of these systems in reducing the vibration responses of long-span bridges and tall buildings exposed to wind loads. For instance, Giaralis et al. [30, 31] examined the effectiveness of utilizing TMDI to alleviate wind-induced vibrations of super-high-rise buildings. It was discovered that the TMDI could effectively reduce structural vibrations without significantly increasing the physical mass. Wang et al.

[32] developed a novel tuned liquid-column-damper-inerter (TLCDI) for controlling wind-induced vibration of connected high-rise buildings and analytically demonstrated that the proposed TLCDI outperformed conventional tuned liquid-column-dampers in terms of reducing the auxiliary mass and suppressing the wind-induced vibrations. Zhu et al. [33] verified that TMDI was superior to the conventional TMD in controlling the dynamic responses of interconnected tall buildings exposed to wind loads, despite the TMDI having only one-third of the auxiliary mass of the traditional TMD. Lu et al. [34] proposed an enhanced particle inerter damper (EPID) by incorporating an inerter element into a conventional particle TMD. It was analytically verified that the proposed EPID was capable of effectively decreasing the seismic-induced responses with a much lower auxiliary mass ratio. KHorsand and Rofooei [35] introduced an innovative auxiliary structure-type TMDI to address the practical challenges associated with the implementation of grounded TMDI, and analytically evaluated its seismic control performance, which was verified to be more effective than traditional retrofitting techniques. Li et al. [36] developed a novel tuned mass damper inerter by repositioning the damping element in the conventional TMDI, and analytically demonstrated that the proposed device could attain better control performance and greater robustness. Su et al. [37] explored the performance of inerter-based double tuned mass dampers (IDTMDs) in suppressing wind-induced vibrations in slender structures. Their findings revealed that the proposed IDTMD could offer superior control effectiveness and weight reduction effect in comparison to conventional TMDs. Said Elias [38] investigated the control performance of distributed tuned mass dampers (D-TMDs) in reducing responses of OWTs subjected to the combined wind and wave loads. It was found that TMDs were more effective in reducing the wind-induced responses rather than wave-induced responses. Similarly, Elias and Beer [39] conducted numerical investigations on multiple tuned mass-damper-inerter systems with electromagnetic motors (TMDI-EM) for vibration control and energy harvesting in offshore wind turbines subjected to wind and wave loads. It was revealed that integrating TMDI-EMs could significantly improve the dynamic characteristics and energy harvesting capability of offshore wind turbines, simultaneously. Dai et al. [40] proposed a Maxwell tuned mass damper inerter (M-TMDI) and investigated its performance in suppressing vortex-induced vibrations in bridges. The results showed that the optimally configured M-TMDI outperformed both traditional TMD and three-element TMD in terms of reducing transient and steady-state amplitudes, limiting stroke, and reducing static stretching. Xu et al. [41] derived the closed-form design formulas specifically for TMDIs to enhance their performances in controlling vortex-induced vibrations in bridges.

Additionally, they also proved that lever-arm TMDI (LTMDI) could be a promising method for mitigating vortex-induced vibrations of long-span bridges [42]. Recent studies [43, 44] have proposed horizontally arranged pendulum-type inerter-based dampers, which can achieve superior performances for reducing crosswind responses of high-rise buildings. Just recently, the authors proposed two nonlinear pendulum tuned mass damper inerters (NPTMDIs) by introducing a vertically arranged "ordinary" or clutched inerter element to conventional PTMDs and verified their superior vibration control performances for tall buildings exposed to earthquake excitations. However, the effectiveness of the two NPTMDIs in mitigating wind-induced vibration responses of high-rise buildings remains uninvestigated.

To bridge this research gap, this study is dedicated to a systematic investigation of the control effectiveness and robustness of NPTMDIs in alleviating the vibration responses of tall buildings under wind loads. The remaining of this study is structured as follows: Section 2 presents two NPTMDIs with different configurations (denoted as NPTMDI I and II) and introduces their working mechanisms; in Section 3, the analytical models of a tall building structure with NPTMDI I and II are established, and the corresponding equations of motion are given; following that, the optimal parameters of NPTMDIs are obtained and shown in Section 4; in Section 5, the vibration control performances of the two NPTMDIs are comprehensively investigated; finally, several key conclusions are highlighted in Section 6.

2. NPTMDIs

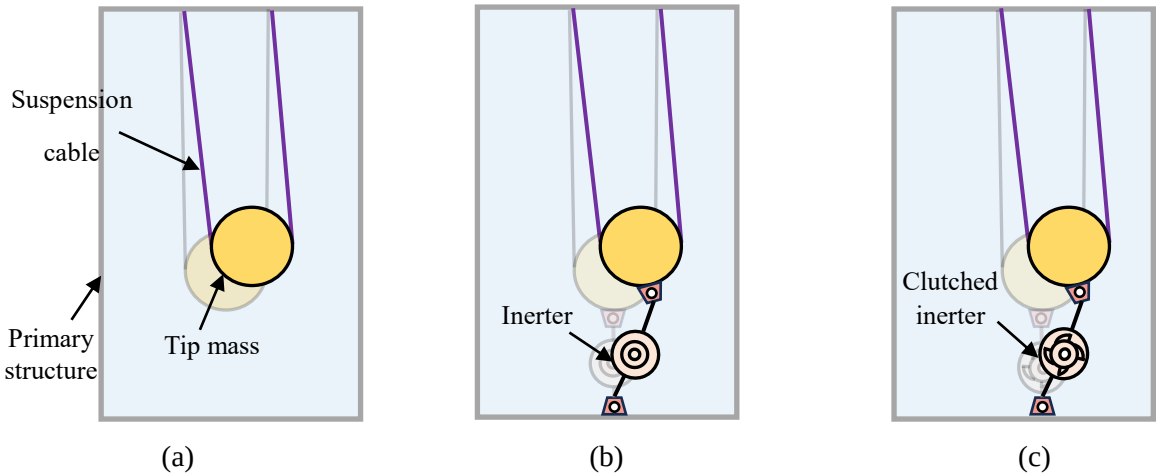

Fig. 1. Schematic drawings of different control systems. (a) Conventional PTMD; (b) NPTMDI I; (c) NPTMDI II

This section offers a comprehensive introduction to the configurations and working mechanisms

of the proposed two NPTMDIs, termed NPTMDI-I and NPTMDI-II. Fig.1 illustrates their schematic drawings, while Fig. 2 shows the working mechanism using NPTMDI I as an example. Besides, for comparison, the schematic of their counterpart, namely the conventional PTMD, is also shown in Fig. 1(a), which mainly consists of a tip mass and a suspension cable. When the primary structure experiences an external force, the tip mass of PTMD will swing in the opposite direction of the motion of the primary structure, hence generating an inertial force that dampens the movement of the structure. As illustrated in Fig. 1(b), NPTMDI-I is mainly composed of a tip mass, a pendulum rod, and an inerter. Compared to the conventional PTMD, the inerter is connected between the tip mass and either the ground or a certain location in the primary structure via hinges. Similar to PTMD, the tip mass of NPTMDI I will swing in the opposite direction of structural movement. In addition, the swinging motion of the tip mass can simultaneously activate the inerter, which will produce an inertial force to reduce the vibration of the primary structure. The inertial forces generated by the inerter contribute to a more substantial damping effect, thereby improving the overall vibration attenuation capabilities of the system [45, 46]. Compared to PTMD, the inerter endows NPTMDI I with the capacity to significantly increase the effective mass and enhance the vibration control effectiveness. Additionally, integrating the inerter can reduce the swing angle of the tip mass, thereby minimizing potential collisions between the tip mass and the primary structure. In addition to the 'ordinary' inerter in NPTMDI I, as demonstrated in Fig. 1(c), another classical type, namely the clutched inerter, is also introduced, forming NPTMDI II. It should be noted that the fundamentals of NPTMDI II are similar to that of NPTMDI I. The only difference lies in that the clutched inerter generates inertial force only when the tip mass deviates away from the equilibrium position and does not generate force when the tip mass moves back. In other words, NPTMDI II operates when the response acceleration and velocity are in the same direction; otherwise, the clutch disengages and produces no force. Previous research (e.g., Refs. [47, 48]) has indicated that the control forces generated by clutched inerters are usually lower than that of 'ordinary' inerters when they are designed with the same inertance. This trait is beneficial for enhancing the stability of the system and extending its operational lifespan. Moreover, a clutched inerter can be physically realized by using mechanisms such as a ratchet and pawl, as presented in the previous study [49]. Furthermore, the potential application scenarios of NPTMDIs can refer to those of PTMD, such as the Taipei 101 building.

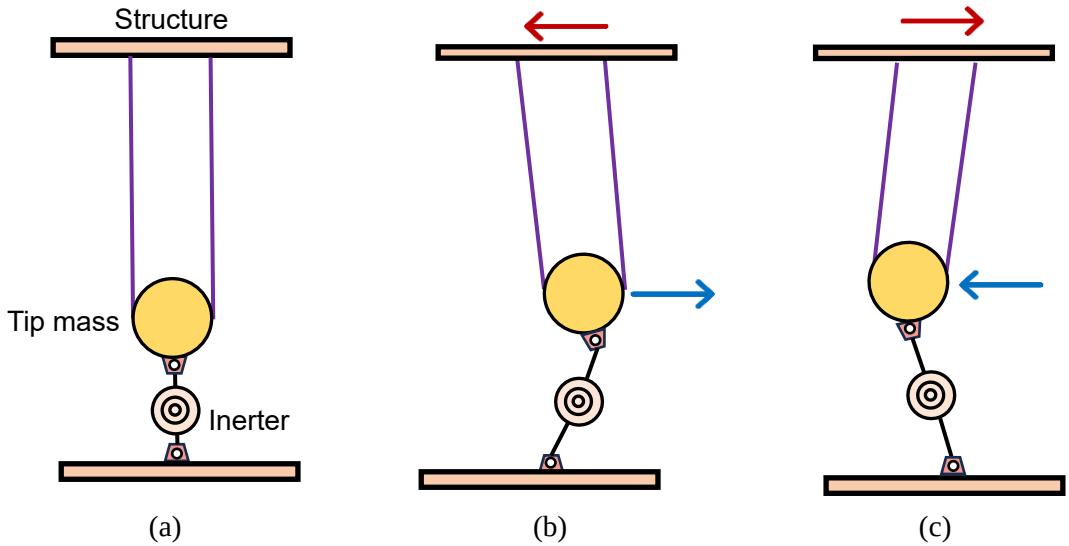

Fig. 2. Flowchart of working mechanism illustrated using NPTMDI I as an example. (a) initial state; (b) leftward movement, (c) rightward movement

3. Analytical models of high-rise buildings equipped with NPTMDIs

After figuring out the working mechanisms of NPTMDIs, a typical slender structure, namely high-rise buildings, is selected as an example, and the analytical models of a high-rise building equipped with NPTMDIs are established in this section. Specifically, a 40-storey benchmark building is chosen to establish the analytical models, and the corresponding equations of motion are formulated. Besides, the calculations of wind loads are also presented.

3.1. Benchmark model

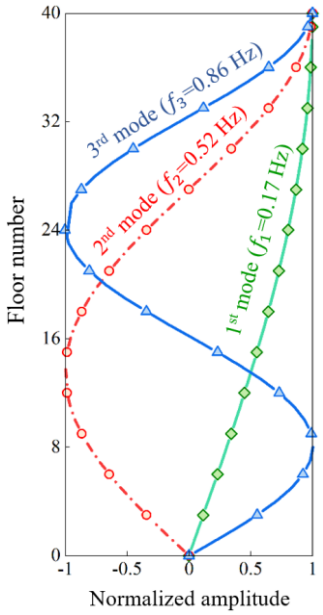

Fig. 3. First three eigenmodes of the 40-storey benchmark building

The adopted 40-storey shear building is from the previous study [50]. Each floor of the building is uniformly constructed with a generalized mass $m_i = 1290$ tons, stiffness $k_i = 10^6$ kN/m, and damping coefficient $c_i = 14260$ kN·s/m, where the subscript $i = 1, 2, \ldots, 40$ denotes the storey index. The first three eigenmodes of the 40-storey benchmark building are depicted in Fig. 3, and its first three fundamental frequencies are 0.17, 0.52, and 0.86 Hz, respectively. More detailed information about this benchmark building can be found in the previous study [50].

3.2. Analytical models

The analytical models of a shear-type 40-storey building equipped with NPTMDIs subjected to wind loads are shown in Fig. 4. Both the control systems (namely NPTMDI I and NPTMDI II) have a tip mass m_a, a pendulum length of l, and a rotational damping coefficient c_m. Additionally, the inerter element in NPTMDIs is with an inertance of b and an original connection length of l_in. As shown in Fig. 4, one end of the inerter element is attached to the j^{th} floor of the primary structure, and the other end is installed to the tip mass m_a. It should be noted that the inerter element in NPTMDI II is a clutched one. In the figure, the displacement response of the i^{th} floor of the building structure relative to the ground is represented by x_i; θ stands for the swing angle of the pendulum rod; and $F_{\mathrm{wind}i}$ denotes the wind load applied to the i^{th} floor of the building.

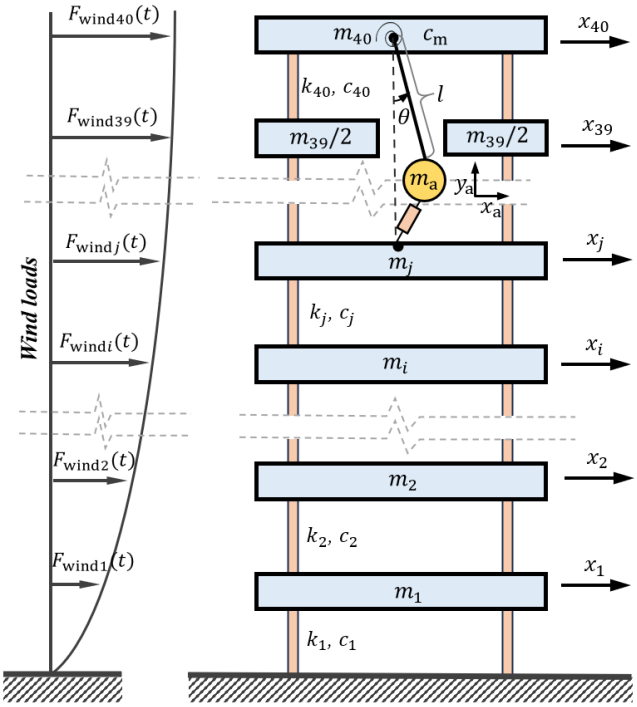

Fig. 4. Analytical models of the 40-storey building with NPTMDIs subjected to wind loads

Based on Fig. 4, the governing equations of motion of a multi-degree-of-freedom (MDOF) structure equipped with NPTMDIs are derived by Lagrange approach. These equations can be described in relation of the system potential energy U, kinetic energy T, and energy dissipation function F as follows:

$$T = T_1 + T_a + T_b = \frac{1}{2}\sum_{i=1}^{40}\frac{1}{2}m_i\dot{x}_i{}^2 + \frac{1}{2}m_a\left(\dot{x}_a{}^2 + \dot{y}_a{}^2\right) + \frac{1}{2}b\dot{x}_b{}^2 \tag{1a}$$

$$U = \frac{1}{2}k_1x_1{}^2 + \frac{1}{2}\sum_{i=2}^{40}\frac{1}{2}k_i(x_i - x_{i-1})^2 + m_agl(1-\cos\theta) \tag{1b}$$

$$F = \frac{1}{2}c_1\dot{x}_1{}^2 + \frac{1}{2}\sum_{i=2}^{40}\frac{1}{2}c_i(\dot{x}_i - \dot{x}_{i-1})^2 + \frac{1}{2}c_m\dot{\theta}^2 \tag{1c}$$

where T_1, T_2, and T_b represent the kinetic energy of the block mass, the tip mass, and inerters, respectively; g is the gravitational acceleration.

According to the geometric relationship of the movement of NPTMDIs, the lateral and vertical displacement of the tip mass, i.e., x_a and y_a, can be expressed as follows:

$$\begin{cases} x_a = x_i + l\sin\theta \\ y_a = l(1-\cos\theta) \end{cases} \tag{2}$$

In Eq. (1a), x_b is the relative displacement between the two ends of the inerter element, which can be mathematically represented as:

$$x_b = \sqrt{\left((x_i - x_j) + l\sin\theta\right)^2 + (l + l_{in} - l\cos\theta)^2} - l_{in} \tag{3}$$

Based on Lagrange's formulation, the equations of motion of the coupled system can be formulated as follows.

$$\frac{d}{dt}\left(\frac{\partial(T-U)}{\partial\dot{x}_1}\right) - \frac{\partial(T-U)}{\partial x_1} + \frac{\partial F}{\partial\dot{x}_1} = Q_1 \tag{4a}$$

$$\frac{d}{dt}\left(\frac{\partial(T-U)}{\partial\dot{\theta}}\right) - \frac{\partial(T-U)}{\partial\theta} + \frac{\partial F}{\partial\dot{\theta}} = Q_2 \tag{4b}$$

in which the over dots denote derivatives in relation to time t; Q_1 and Q_2 represent the generalized forces of the primary structure and NPTMDIs, respectively.

To streamline the analysis and computational complexity associated with the equations above and facilitate more efficient analysis, the rotational angles of NPTMDIs are assumed small, and $\sin\theta$ and $\cos\theta$ thus can be approximated as θ and 1, respectively. It is important to note that this assumption is deemed reasonable because the involvement of inerter could reduce the vibration amplitude of the control device as revealed in many previous studies (e.g., Ref. [51]).

Subsequently, substituting Eqs. (1)-(3) into Eq. (4), the equation that governs the dynamics of the high-rise building equipped with NPTMDI I can be described as follows:

$$\boldsymbol{M_s}\ddot{\boldsymbol{X}}_s + \boldsymbol{C_s}\dot{\boldsymbol{X}}_s + \boldsymbol{K_s}\boldsymbol{X_s} + \boldsymbol{F_I} = \boldsymbol{F}_{\text{wind}} \tag{5}$$

where

$$\boldsymbol{M_s} = \begin{bmatrix} \boldsymbol{M_{40\times40}} + m\boldsymbol{D_1}\boldsymbol{D_1}^{\text{T}} & ml\boldsymbol{D_1} \\ ml\boldsymbol{D_1}^{\text{T}} & ml^2 \end{bmatrix} \tag{6a}$$

$$\boldsymbol{C_s} = \begin{bmatrix} \boldsymbol{C_{40\times40}} & 0 \\ 0 & c_{\text{m}} \end{bmatrix} \tag{6b}$$

$$\boldsymbol{K_s} = \begin{bmatrix} \boldsymbol{K_{40\times40}} & 0 \\ 0 & mgl \end{bmatrix} \tag{6c}$$

in which $\boldsymbol{M_s}$, $\boldsymbol{K_s}$ and $\boldsymbol{C_s}$ denote the mass, stiffness, and damping matrices of the high-rise building equipped with different control systems, respectively; $\boldsymbol{M_{40\times40}}$, $\boldsymbol{K_{40\times40}}$ and $\boldsymbol{C_{40\times40}}$ represent the corresponding matrices of the high-rise building without control, respectively; c_{m} denotes the rotational damping coefficient of NPTMDIs; $\boldsymbol{X_s} = [x_1, x_2, \dots, x_{40}, \theta]^{\text{T}}$ is the displacement vector, where θ stands for the angular rotation of the tip mass; $\boldsymbol{D_1}$ is the location vector of the tip mass; and $\boldsymbol{F}_{\text{wind}} = [F_{\text{wind1}}, F_{\text{wind2}}, \dots, F_{\text{wind40}}]$ represents the wind load vector.

In Eq. (5), $\boldsymbol{F_I}$ is the inertial force generated by NPTMDIs, which can be calculated by

$$\boldsymbol{F_I} = \begin{bmatrix} \boldsymbol{A_{11}} & \boldsymbol{A_{12}} \\ \boldsymbol{A_{21}} & \boldsymbol{A_{22}} \end{bmatrix} \ddot{\boldsymbol{X}}_s \tag{7}$$

where $\boldsymbol{A_{11}}$, $\boldsymbol{A_{12}}$, $\boldsymbol{A_{21}}$, and $\boldsymbol{A_{22}}$ are the coupling matrices, which are given by Eq. (8).

$$\boldsymbol{A_{11}} = \frac{((x_i - x_j) + l\theta)^2}{{l_{\text{in}}}^2 + ((x_i - x_j) + l\theta)^2}\boldsymbol{D_2}\boldsymbol{D_2}^{\text{T}}b \tag{8a}$$

$$\boldsymbol{A_{12}} = \frac{((x_i - x_j) + l\theta)((l + l_{\text{in}})\theta + (x_i - x_j))l}{{l_{\text{in}}}^2 + ((x_i - x_j) + l\theta)^2}\boldsymbol{D_2}b \tag{8b}$$

$$\boldsymbol{A_{21}} = \frac{((x_i - x_j) + l\theta)((l + l_{\text{in}})\theta + (x_i - x_j))l}{{l_{\text{in}}}^2 + ((x_i - x_j) + l\theta)^2}\boldsymbol{D_2}^{\text{T}}b \tag{8c}$$

$$\boldsymbol{A_{22}} = \frac{((l + l_{\text{in}})\theta + (x_i - x_j))^2 l^2}{{l_{\text{in}}}^2 + ((x_i - x_j) + l\theta)^2}b \tag{8d}$$

in which $\boldsymbol{D_2}$ is the location vector of the inerter element.

It should be noted that, as shown in Fig. 1(c), the NPTMDI II can provide control force only when its clutched inerter undergoes the deceleration phase (namely $\dot{x}_{\text{b}}\ddot{x}_{\text{b}} < 0$). Thus, the control force of NPTMDI II system can be calculated by Eq. (9), and its equation of motion can be obtained

by replacing $\boldsymbol{F}_{\mathbf{I}}$ in Eq. (5) with $\boldsymbol{F}_{\mathbf{II}}$.

$$\boldsymbol{F}_{\mathbf{II}} = \begin{cases} \boldsymbol{F}_{\mathbf{I}} & \text{when } \dot{x}_{\mathrm{b}}\ddot{x}_{\mathrm{b}} < 0 \\ \mathbf{0} & \text{when } \dot{x}_{\mathrm{b}}\ddot{x}_{\mathrm{b}} \geq 0 \end{cases} \tag{9}$$

For comparison, the scenario of the primary structure equipped with PTMD is also analysed, and the corresponding equation of motion can be obtained by setting b in Eq. (5) to zero.

3.3. Calculation of wind loads

The subsequent step is to calculate the wind loads that are applied to the benchmark model. It is well recognized that the wind loads acting on a high-rise building vary along the height, which can be decomposed into a constant mean wind load and a fluctuating wind load component. For the fluctuating wind load, the widely used Kaimal spectrum [52, 53] is adopted to model the power spectral density (PSD) function of the wind velocity along the height of the building, which is shown below.

$$S_{\mathrm{vv}}(y,f) = \frac{v_*^2}{f}\frac{200\hat{c}}{(1+50\hat{c})^{5/3}} \tag{10}$$

$$\hat{c} = fy/\bar{v}(y) \tag{11}$$

$$\bar{v}(y) = v_* \ln(y/y_0)K \tag{12}$$

in which f denotes frequency (Hz); v_* represents the friction velocity; $\hat{c}$ stands for the Monin coordinate; y represents the vertical coordinate of the i^{th} floor; y_0 is the roughness length; and K represents the von-Karman's constant.

After determining the PSD of wind velocity, as Eq. (13) shows, by summing up the contributions of all frequency components using the trigonometric superposition method, the fluctuating wind velocity can be determined.

$$v_{\mathrm{f}} = \sum_{i=1}^{N/2} \sqrt{2S_{\mathrm{vv}}/T} \times \cos(2\pi f t - \emptyset) \tag{13}$$

where v_{f} is fluctuating wind velocity; T is the randomly selected period points; t represents time; and $\emptyset$ stands for the corresponding phase.

The total wind velocity v_{total} corresponding to the i^{th} floor is therefore expressed as follows:

$$v_{\mathrm{total}} = v_{\mathrm{mean}} + v_{\mathrm{f}} \tag{14}$$

in which v_{mean} represents mean velocity.

Finally, the wind load applied to the i^{th} floor can be calculated by

$$F_{\text{wind}i} = \frac{1}{2}\rho A_i C_{\text{d}} v_{\text{total}}^2 \tag{15}$$

where ρ is air density; A_i represents the corresponding projected area of the i^{th} floor; C_{d} stands for the drag coefficient.

In the simulation, the parameters are configured as follows: the roughness length $y_0 = 0.005$, air density $\rho = 1.25$ kg/m^3, drag coefficient $C_{\text{d}} = 1.2$, and the average wind velocity at the height of 120 m is set to 18.6 m/s. In addition, the benchmark building is divided into 40 segments for calculating the wind loads which are then exerted on the corresponding degrees of freedom. Since the adopted benchmark building is an analytical model without specific design details, the windshield of each floor is assumed to be the same, i.e., 300 m^2. Fig. 5(a) shows the power spectrum of fluctuating wind velocity at the height of 60 m. As can be seen, the simulated spectrum aligns well with the target spectrum, which verifies the accuracy of wind load simulation. Fig. 5(b) shows the time history of the simulated wind load exerted on the building at the height of 120 m.

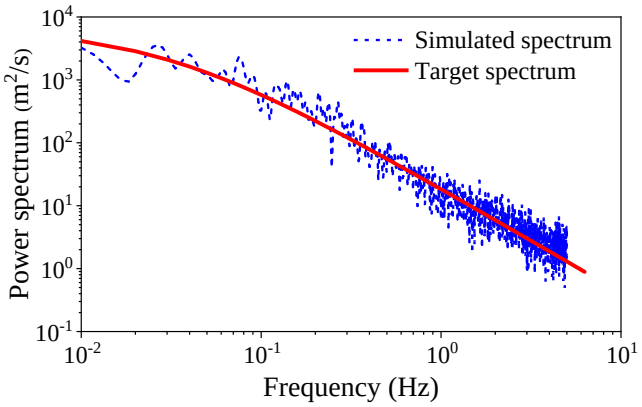

(a)

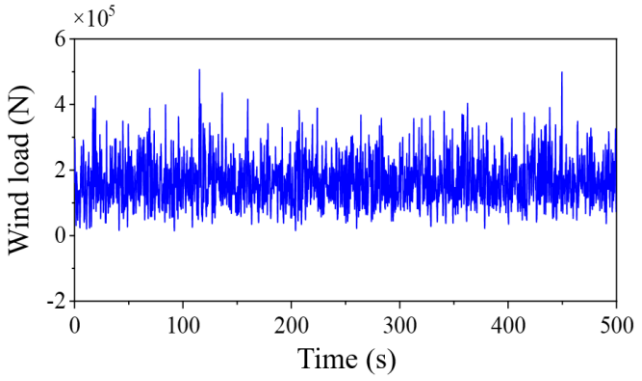

(b)

Fig. 5. Generated wind load. (a) spectra comparison; (b) time history

4. Optimization

For tuning control systems, an effective optimization method is crucial for achieving efficient vibration control performance. As detailed in Section 3, the equations of motion of the building structure incorporating the proposed NPTMDIs include multiple nonlinear terms. These nonlinear terms render it challenging and time-intensive to formulate the mathematical expressions of the optimal parameters of NPTMDIs. Consequently, in this study, advanced algorithm-based numerical optimization methods, such as genetic algorithms, are adopted to determine the optimal parameters. Moreover, to streamline the optimization process, the generalized 2-degree-of-freedom analytical models of the primary structure equipped with NPTMDIs are developed based on previous studies, e.g., Refs. [54, 55], which are shown in Fig. 6.

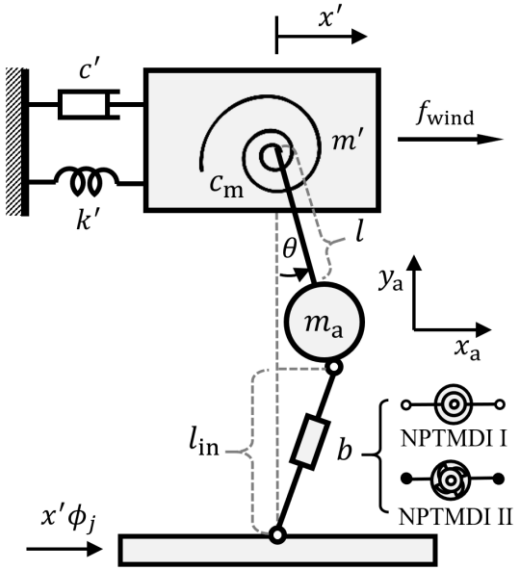

Fig. 6. Simplified benchmark model equipped with NPTMDIs

As Fig. 6 illustrates, since the responses of the tall building subjected to wind loads are generally governed by the first mode, it is modeled by a mass block $m' = \boldsymbol{\phi}^T \boldsymbol{M}_{40\times40}\boldsymbol{\phi}$, which is attached to the ground through a spring $k' = \boldsymbol{\phi}^T \boldsymbol{K}_{40\times40}\boldsymbol{\phi}$ and a dashpot $c' = \boldsymbol{\phi}^T \boldsymbol{C}_{40\times40}\boldsymbol{\phi}$. Moreover, one end of the inerter element in the NPTMDIs is attached to the j^{th} floor of the structure with modal displacement ϕ_j, and the other end is attached to the tip mass m_a which is then connected to the mass block thorough a suspension cable of length l. Herein, $\boldsymbol{\phi}$ denotes the mode shape vector for a specific vibration mode; x' stands for the displacement of the top floor of the building structure relative to the ground; θ represents the swing angle of the pendulum rod; and f_{wind} is the total wind load, which is randomly generated and has a duration of 800 s. The definitions of other

parameters are consistent with those presented in subsection 3.2.

To generalize the results and simplify the subsequent optimization process, the following non-dimensional parameters are defined:

$$\mu = \frac{m_{\mathrm{a}}}{m'} \tag{16a}$$

$$\beta = \frac{b}{m'} \tag{16b}$$

$$\gamma = \frac{\omega_2}{\omega_1} \tag{16c}$$

$$\delta = \frac{l_{\mathrm{in}}}{l} \tag{16d}$$

$$\xi_1 = \frac{c'}{2m'\omega_1} \tag{16e}$$

$$\xi_2 = \frac{c_{\mathrm{m}}}{2m_{\mathrm{a}}l^2\omega_2} \tag{16f}$$

in which μ represents the mass ratio of NPTMDIs (or PTMD); β is the inertance-to-mass ratio of NPTMDIs; γ is the frequency ratio of NPTMDIs (or PTMD); δ is the connection length ratio of NPTMDIs; ξ_1 and ξ_2 denote the damping ratios of the primary structure and NPTMDIs (or PTMD), respectively; and ω_1 and ω_2 stand for the natural frequency of the primary structure and frequencies of NPTMDIs, respectively, which can be calculated by

$$\omega_1 = \sqrt{\frac{k'}{m'}} \tag{17a}$$

$$\omega_2 = \sqrt{\frac{\mathrm{g}}{l}} \tag{17b}$$

According to the previous study, i.e., Ref. [50], the mass ratio μ of the system selected for analysis is set to 0.5%, and its damping ratio ξ_1 is set to 0.77%. Eq. (18) summarizes the optimization problem. As can be seen, the optimization objective is to minimize the peak top-floor acceleration. Optimization variables include the tuning ratio γ, the inertance-to-mass ratio β, the connection length ratio δ, and the damping ratio ξ_2, the respective ranges of which are given below.

$$\begin{gathered} \text{minimize } \psi\ (\gamma, \xi_2, \beta, \delta) \\ \text{subjected to } \gamma\epsilon(0,5], \xi_2\epsilon(0,1], \beta\epsilon(0,0.2], \delta\epsilon[0.1,1] \\ \psi = \max|\ddot{x}'| \end{gathered} \tag{18}$$

Notably, the optimization would be repeatedly processed ten times, and the mean values of all optimization outcomes are taken as the final optimal parameters to minimize potential bias.

For the optimization of PTMD, the closed-form expressions of its optimal parameters provided

in the previous study [56] are utilized, which are also given below

$$\gamma_{\text{opt}} = \frac{1}{\sqrt{1+\mu}}$$
$$\xi_{\text{opt}} = \frac{3\mu}{8(1+\frac{\mu}{2})} \tag{19}$$

It should be noted that the closed-form solutions for the optimal parameters of PTMD are used in this study due to their simplicity and efficiency. Although derived for undamped systems, they remain sufficiently accurate for estimating the optimal parameters of PTMD applied in structures with relatively low damping ratios.

Table 1 outlines the optimal parameters of PTMD, NPTMDI I, and NPTMDI II under the condition of mass ratio $\mu = 0.5\%$ and damping ratio $\xi_1 = 0.77\%$. As can be seen, the optimal values of β and δ of NPTMDIs reach the upper and lower bounds of their predefined ranges, respectively, indicating that within the given variable ranges, the higher the value of β and/or the lower the value of δ, the more significant the control effect of NPTMDIs.

Table 1 Optimal parameters of PTMD, NPTMDI I, and NPTMDI II

Control systems	γ_{opt}	$\xi_{2\text{opt}}$	β_{opt}	δ_{opt}
PTMD	0.99	0.01	N/A	N/A
NPTMDI-I	1.76	0.38	0.20	0.10
NPTMDI-II	1.23	0.36	0.20	0.10

*N/A: not appliable

5. Effectiveness and robustness analyses

5.1. Control effectiveness of NPTMDIs

Based on the obtained optimal parameters, the time histories of the top-floor displacement and acceleration responses of the high-rise building equipped with PTMD, NPTMDI I, and NPTMDI II under wind load are obtained and shown in Figs. 7 and 8, respectively. It should be noted that the inerter elements in the two NPTMDIs are all attached to the 30$^{\text{th}}$ floor of the building structure. For comparison, the results of the uncontrolled high-rise building are also given. According to these figures, the following phenomenon can be noted: (1) all control systems, namely PTMD, NPTMDI I, and NPTMDI II, can effectively mitigate the responses of the building structure; (2) the vibration

control effectiveness of the three systems can be ranked in the following descending order: NPTMDI I, NPTMDI II, and PTMD. The improved performances of the proposed NPTMDIs are attributed to the inclusion of the inerter elements because they can significantly enhance the control forces of the control systems. Additionally, in comparison to the clutched inerter used in NPTMDI II, the "ordinary" inerter in NPTMDI I can provide resisting force throughout all stages of motion, which thereby contributes to greater energy dissipation capacity and better vibration control performance.

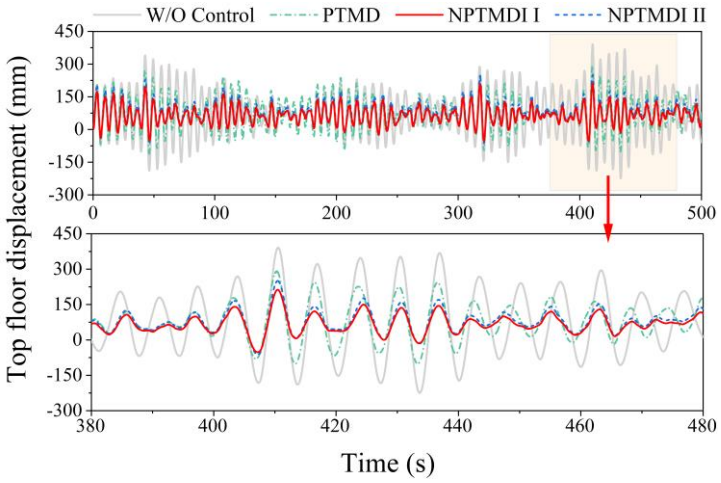

Fig. 7. Top-floor displacement time histories of the high-rise building with PTMD, NPTMDI I, and NPTMDI II systems

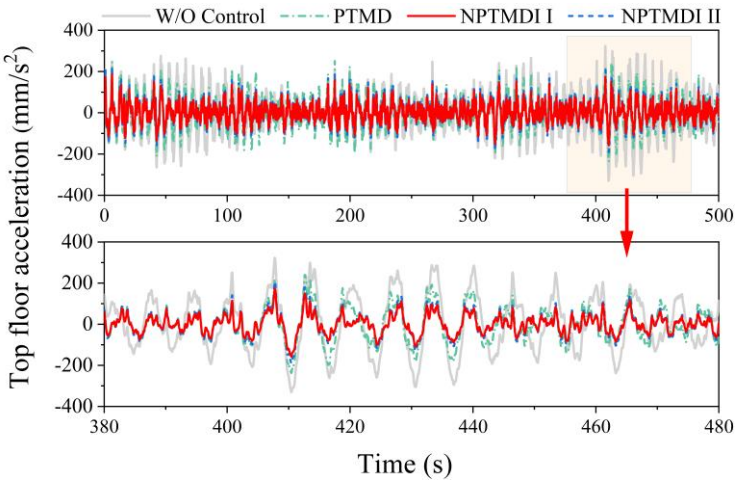

Fig. 8. Top-floor acceleration time histories of the high-rise building with PTMD, NPTMDI I, and NPTMDI II systems

Moreover, the displacement histories of the tip mass are also obtained and shown in Fig. 9. The results indicate that, in comparison to PTMD, the employment of the nonlinearly arranged inerter elements endows NPTMDIs the capacities to effectively mitigate the displacement response of the tip mass. Besides, NPTMDI I demonstrates superior performance than NPTMDI II in diminishing the response of tip mass. In particular, the peak displacement response of the tip mass of PTMD is

1759.96 mm, while that of NPTMDI I and NPTMDI II are only 603.03 mm and 966.47 mm, respectively. It is notable that the maximum displacement observed in Fig. 9, i.e., 1759.96 mm of PTMD, corresponds to the swing angle of 6º, which is consistent with the small angle assumption made during the derivation process. Therefore, the proposed NPTMDIs are more reliable, because they can significantly lower the risk of collision between the auxiliary mass and the structure.

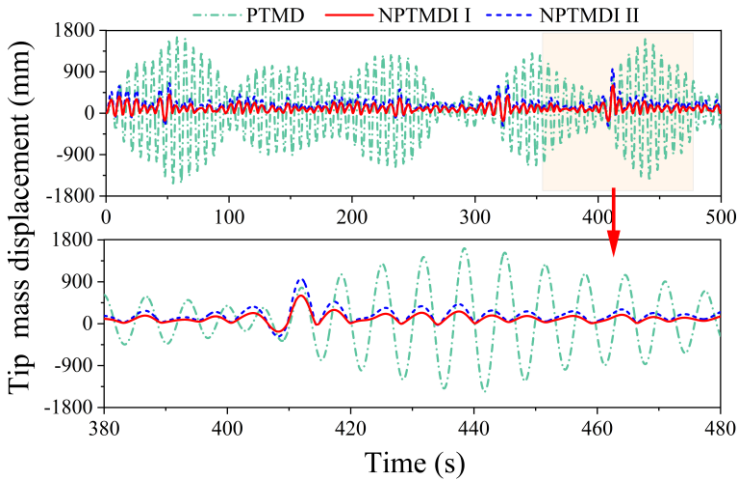

Fig. 9. Displacement time histories of the tip mass in PTMD, NPTMDI I, and NPTMDI II systems

To quantitively evaluate the performances of these three control systems, a response reduction ratio is defined as Eq. (20).

$$\varphi = \frac{\lambda_{\mathrm{u}} - \lambda_{\mathrm{c}}}{\lambda_{\mathrm{u}}} \times 100\% \tag{20}$$

where λ_{c} represents the responses of the structure with control systems; and λ_{u} denotes the corresponding responses of the uncontrolled structure.

Table 2 and Table 3 tabulate the RMS and peak values of the top-floor displacement and acceleration responses of the high-rise building without control and with PTMD, NPTMDI I, and NPTMDI II systems, as well as the corresponding response reduction ratios of these three control systems, respectively. As shown, the response reduction ratios of PTMD, NPTMDI I, and NPTMDI II systems are all greater than 0, which means that they can effectively mitigate the displacement and acceleration responses of the high-rise building. Moreover, as the results show, introducing inerter elements to PTMD to form NPTMDIs can obviously improve the vibration control performances, and the “ordinary” inerter performs better than the clutched one. Take the peak top-floor responses presented in Table 3 as an illustrative example, the peak displacement response of the structure without control is 391.16 mm, while that of the scenario with PTMD, NPTMDI I, and NPTMDI II systems are 291.38 mm, 212.75 mm, and 250.26 mm, respectively, and the corresponding response

reduction ratios are 25.51%, 45.61% and 36.02%, respectively. As for the peak acceleration response, it is 331.67 mm/s^2 for the uncontrolled structure. With the implementation of PTMD, NPTMDI I, and NPTMDI II, the response is reduced to 251.67 mm/s^2, 183.05 mm/s^2, and 217.97 mm/s^2, respectively. The corresponding reduction ratios φ are 24.12%, 44.81%, and 34.28%, respectively, which further verifies the effectiveness of the proposed NPTMDIs in controlling wind-induced vibrations of high-rise buildings.

Table 2 Comparison between the RMS top-floor responses of different control systems

Control systems	Values		φ (%)	
	Dis. (mm)	Acc. (mm/s^2)	Dis.	Acc.
W/o control	141.72	112.66	N/A	N/A
PTMD	110.63	76.12	21.93	32.43
NPTMDI I	80.43	54.81	43.25	51.35
NPTMDI II	95.36	56.08	32.71	50.22

*N/A: not applicable

Table 3 Comparison between the peak top-floor responses of different control systems

Control systems	Values		φ (%)	
	Dis. (mm)	Acc. (mm/s^2)	Dis.	Acc.
W/o control	391.16	331.67	N/A	N/A
PTMD	291.38	251.67	25.51	24.12
NPTMDI I	212.75	183.05	45.61	44.81
NPTMDI II	250.26	217.97	36.02	34.28

*N/A: not applicable

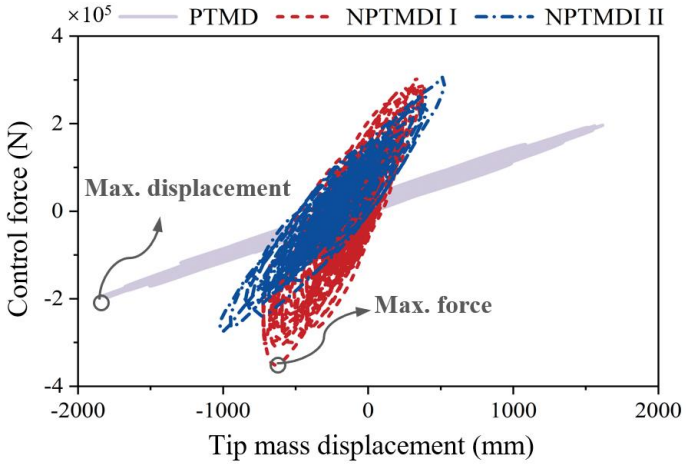

Fig. 10. Hysteretic curves of PTMD, NPMTDIs I and II subjected to wind loads

To provide a deeper insight into the performances, Fig. 10 illustrates the wind-induced hysteretic

curves of different control systems, specifically the relationship between the tip mass displacement and the control force. The maximum control force magnitudes are ranked as follows: NPTMDI I > NPTMDI II > PTMD, while the maximum tip mass displacement follows the order: PTMD > NPTMDI II > NPTMDI I. These results indicate that incorporating either the "ordinary" or the clutched inerter can reduce the swing angle of the tip mass while increasing the control force. It is also found that the "ordinary" inerter could generate a larger control force and smaller displacement of the tip mass in comparison to the clutched inerter. Furthermore, the areas enclosed within the hysteretic curves of NPTMDI I and II are significantly greater than that of the conventional PTMD, highlighting the superior energy dissipation capabilities of the proposed NPTMDIs. This enhanced performance explains why the NPTMDIs outperform the conventional PTMD.

Furthermore, there exist strong uncertainties in wind velocity parameters, and their influences on the control effectiveness of NPTMDIs should be well addressed. Given this fact, the control effectiveness of NPTMDIs under different wind velocities is further examined. Fig. 11 illustrates the normalized peak displacement and acceleration responses of the tall building equipped with different control systems subjected to wind loads with different velocities. In this figure, the wind velocity refers to the wind velocity at the top floor, which is assumed to range from 10 m/s to 50 m/s, and the results are normalized by using the corresponding maximum response of the uncontrolled structure. As illustrated, the normalized responses of the high-rise building with different control systems increase almost linearly with the wind velocity. However, both NPTMDI I and II outperform the conventional PTMD regardless of the wind velocity, further demonstrating the performance improvements due to the incorporation of inerter.

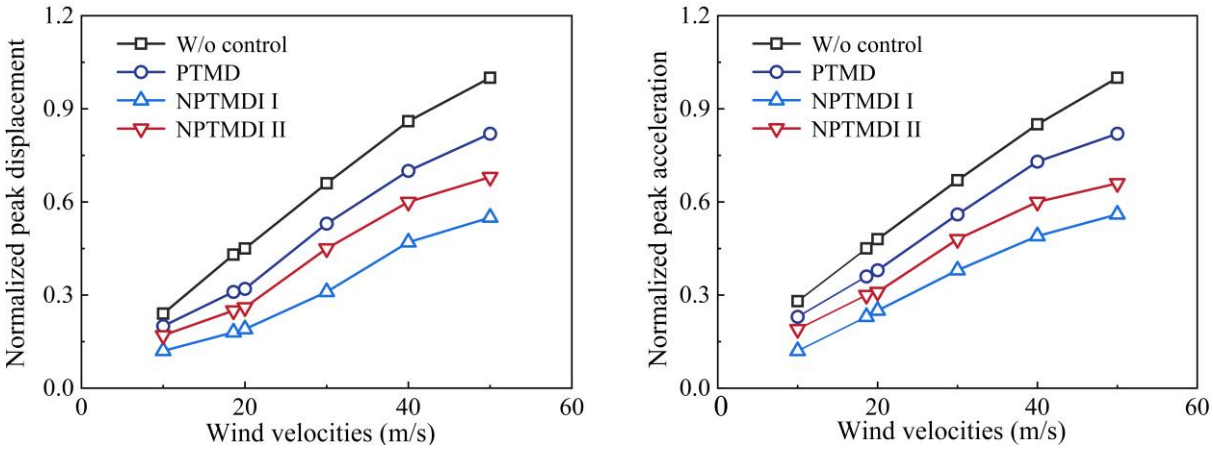

Fig. 11. Normalized responses of the high-rise building with different control systems under different velocities. (a) normalized peak displacement; (b) normalized peak acceleration

5.2. Influence of the installation locations of NPTMDIs

Fig. 12 presents the peak responses of each floor in the high-rise building equipped with NPTMDI I that is installed on different locations. As observed, in contrast to the structure without control, whether NPTMDI I is installed on the 10th, 20th, or 30th floor, it can significantly reduce the peak top-floor displacement and acceleration responses of the building structure simultaneously. The corresponding results of the scenario with NPTMDI II are shown in Fig. 13, which can also achieve significant vibration mitigation effects no matter which floor it is installed on. More importantly, the vibration control effectiveness of both NPTMDI I and II is enhanced as their installation floors decrease. This is because the force generated by an inerter element is related to the relative acceleration between its two connection points. As the connection floor decreases, the relative acceleration between the two ends of the inerter will be amplified, which can contribute to greater control forces and hence realize a more significant vibration mitigation effect. Although the peak top-floor displacement and acceleration responses are smallest when NPTMDIs are attached to the 10th floor of the building, it inevitably increases the installation space, as well as processing difficulties and costs, which need to be further considered. Therefore, in practical engineering applications, the key to selecting the installation locations of inerters is how to balance the contradiction between control effectiveness and the space occupied and costs.

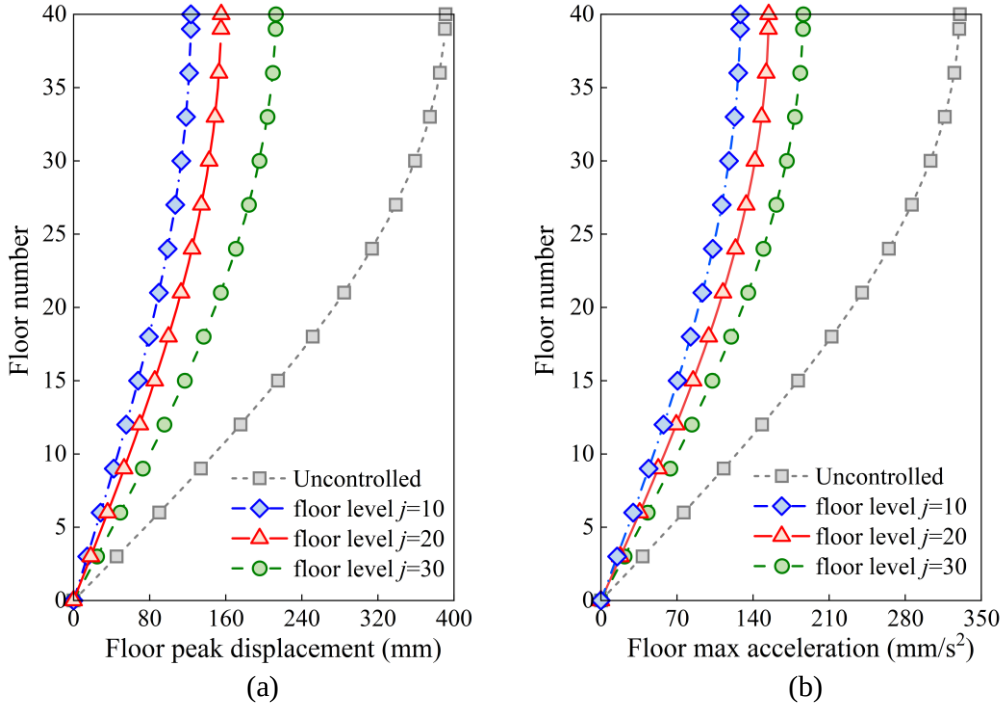

Fig. 12. Peak responses of each floor of the 40-storey building equipped with NPTMDI I installed on different floors. (a) Floor peak displacement (mm); (b) Floor peak acceleration (mm/s^2)

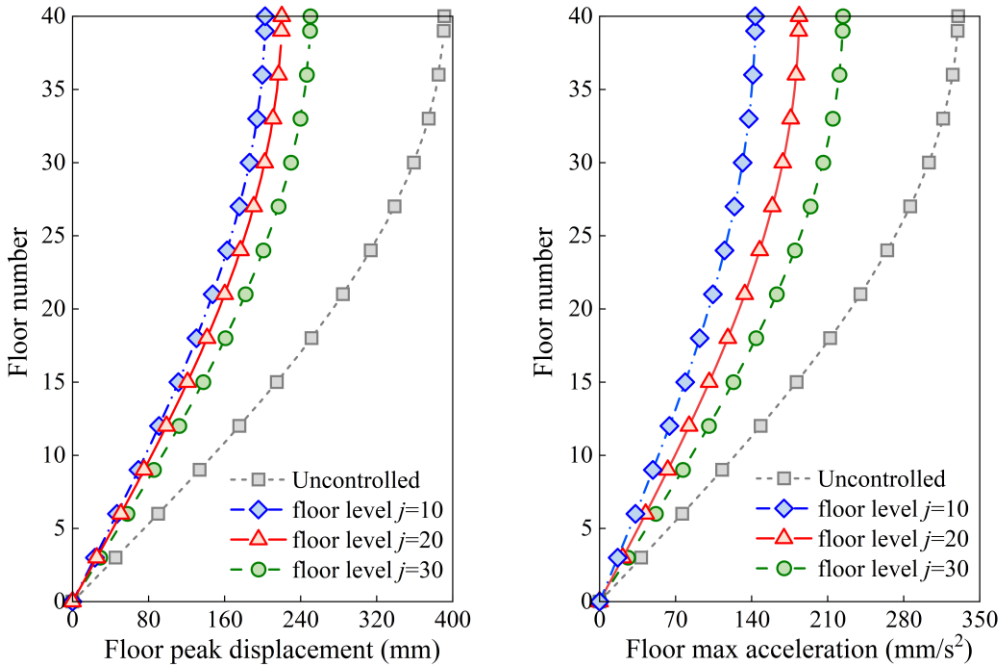

Fig. 13. Peak responses of each floor of the 40-storey building equipped with NPTMDI II installed on different floors. (a) Floor peak displacement (mm); (b) Floor peak acceleration (mm/s^2)

5.3. *Robustness of NPTMDIs against structural uncertainties*

In practice, due to fatigue, environmental corrosion, etc., the structural parameters may deviate from their pre-designed values, which can cause performance degradation of the proposed NPTMDIs. Therefore, a parameter sensitivity analysis is undertaken to evaluate the robustness of NPTMDIs. After imposing a 20% fluctuation up and down on the stiffness and damping coefficients of the primary structure, the reduction ratios of peak top-floor displacement and acceleration responses of PTMD, NPTMDI I, and NPTMDI II systems are obtained and shown in Fig. 14 to Fig. 16. As the figures show, the fluctuations of structural stiffness and damping coefficient can decrease the vibration control performances of PTMD, NPTMDI I, and NPTMDI II systems. Notably, a negative value of φ indicates that the structural responses are not only unsuppressed but also amplified. According to Fig. 14(b), it is able to be found that as structural stiffness and damping coefficients fluctuate up and down by 20%, the minimum and maximum reduction ratios of peak top-floor acceleration of the PTMD system are -9.8% and 24.1%, respectively, resulting in a variation range of 33.9%. Besides, the negative reduction ratio also indicates that introducing the PTMD system to the building structure will amplify the responses when the structural parameters deviate from the pre-designed values. Comparatively, as Figs. 15(b) and 16(b) indicate, the reduction ratios of peak top-

floor acceleration of the NPTMDI I and NPTMDI II systems are all larger than zero, and their variation ranges are 25.3% and 20.0%, respectively, which are significantly lower than that of the PTMD system. Similar results can be obtained from the reduction ratios of peak displacement response illustrated in Figs. 14(a), 15(a), and 16(a). Therefore, it can be concluded that the developed NPTMDIs are more robust to the variations of structural stiffness and damping coefficient than PTMD, which reveals that the employment of inerter element is beneficial for enhancing the robustness of the control system against structural uncertainties.

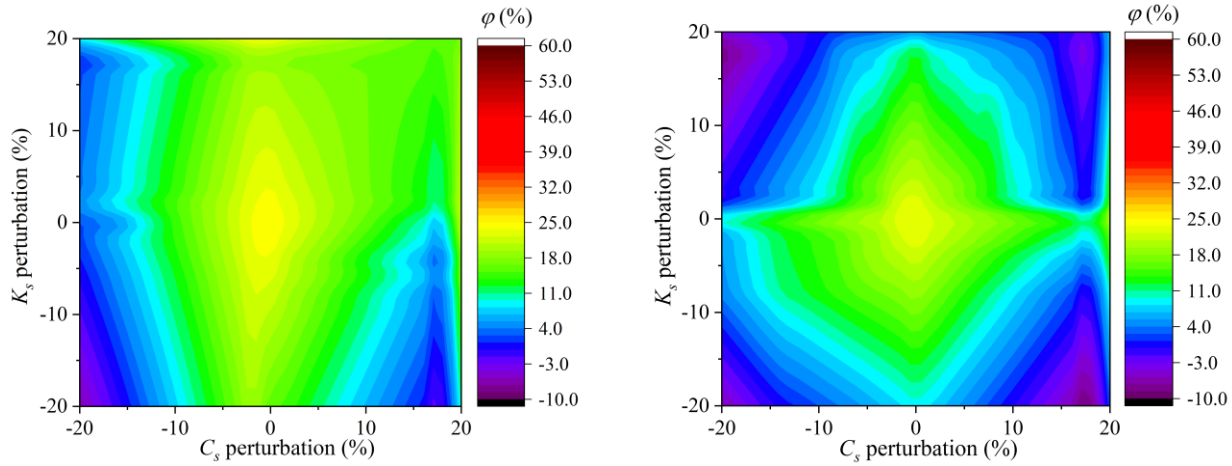

(a) (b)

Fig. 14. Top-floor response reduction ratios of PTMD system under the simultaneous variations of structural stiffness and damping coefficient. (a) Reduction ratios of peak displacement; (b) Reduction ratios of peak acceleration

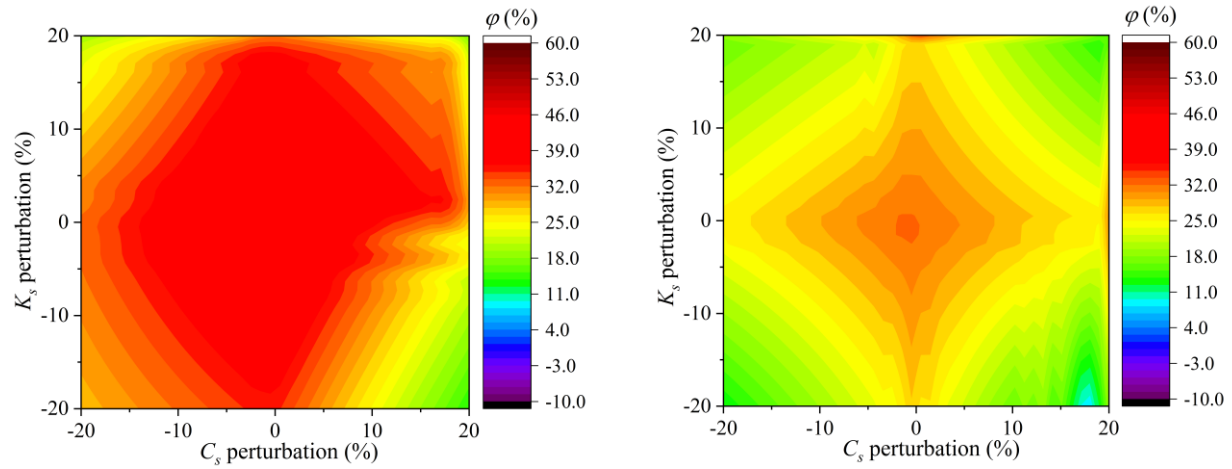

(a) (b)

Fig. 15. Top-floor response reduction ratios of NPTMDI I system under the simultaneous variations of structural stiffness and damping coefficient. (a) Reduction ratios of peak displacement; (b) Reduction ratios of peak acceleration

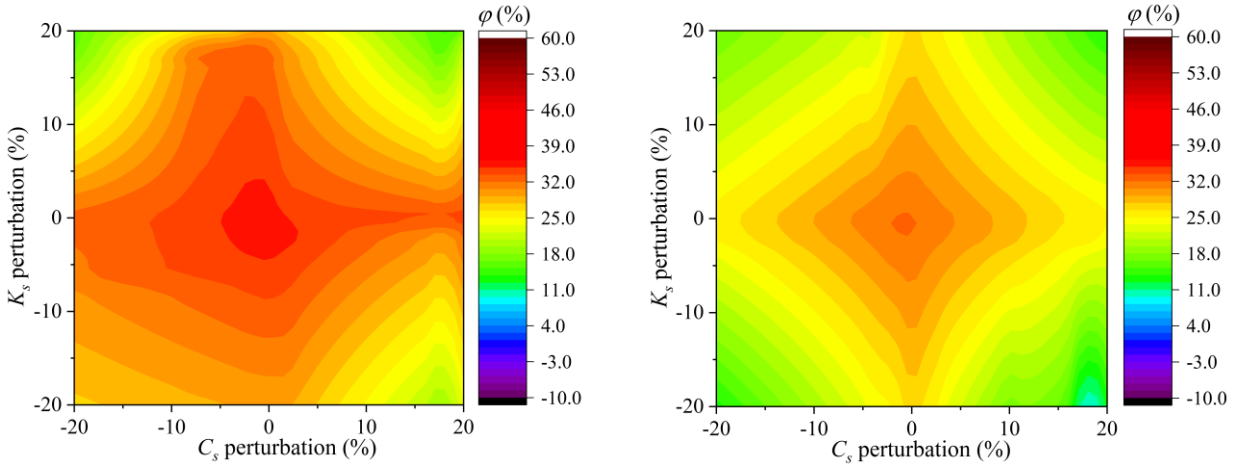

(a) (b)

Fig. 16. Top-floor response reduction ratios of NPTMDI II system under the simultaneous variations of structural stiffness and damping coefficient. (a) Reduction ratios of peak displacement; (b) Reduction ratios of peak acceleration

5.4. *Robustness of NPTMDIs against device uncertainties*

The robustness of NPTMDIs against the uncertainties of structural parameters was verified in the previous subsection. However, in engineering applications, the design parameters of the devices may also deviate from their intended values because of manufacturing and installation errors. To address this issue, the robustness of NPTMDIs with respect to the uncertainties existing in their own structural parameters is further investigated in this subsection. Figs. 17 and 18 illustrate the top-floor response reduction ratios of various control systems under the perturbations of tuning ratio γ and damping ratio ξ_2, respectively. In these figures, γ and ξ_2 are assumed to fluctuate in the range of -20%~20%, and Max, Min and Ω represent the maximum, minimum, and median reduction ratios, respectively. Based on these figures, some overall observations can be made: (1) the perturbations of the device parameters could reduce the effectiveness of PTMD, NPTMDI I and II; (2) compared to the PTMD, the proposed NPTMDIs have stronger robustness against device uncertainties. More specifically, take the perturbation of γ as an example (i.e., Fig. 17(a)), the minimum and maximum reduction ratios of the peak top-floor displacement of the PTMD system are 3.3% and 25.5%, respectively, and the variation range is 22.2%. Comparatively, the variation ranges of the NPTMDI I and NPTMDI II systems are 20.8% and 15.9%, respectively, which are lower than that of the PTMD system. Similar results can also be observed in Fig. 18. Take the peak acceleration as the illustrative example, the minimum and maximum reduction ratios of the peak top-floor acceleration of the PTMD

system are 5.2% and 24.3%, respectively, and the variation range is 19.1%, which is higher than those of NPTMDI I and II. Furthermore, even with parameter perturbations, the median reduction ratios Ω of these three control systems consistently follow the order: NPTMDI I > NPTMDI II > PTMD, further verifying the excellent control performance of the developed NPTMDIs.

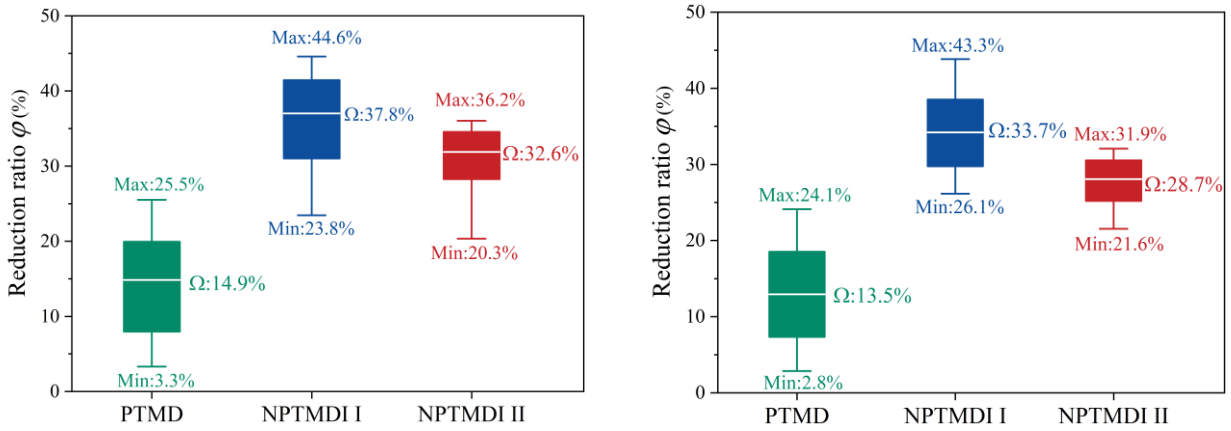

(a) (b)

Fig. 17. Top-floor response reduction ratios of different systems under perturbations of γ. (a) Reduction ratios of peak displacement; (b) Reduction ratios of peak acceleration

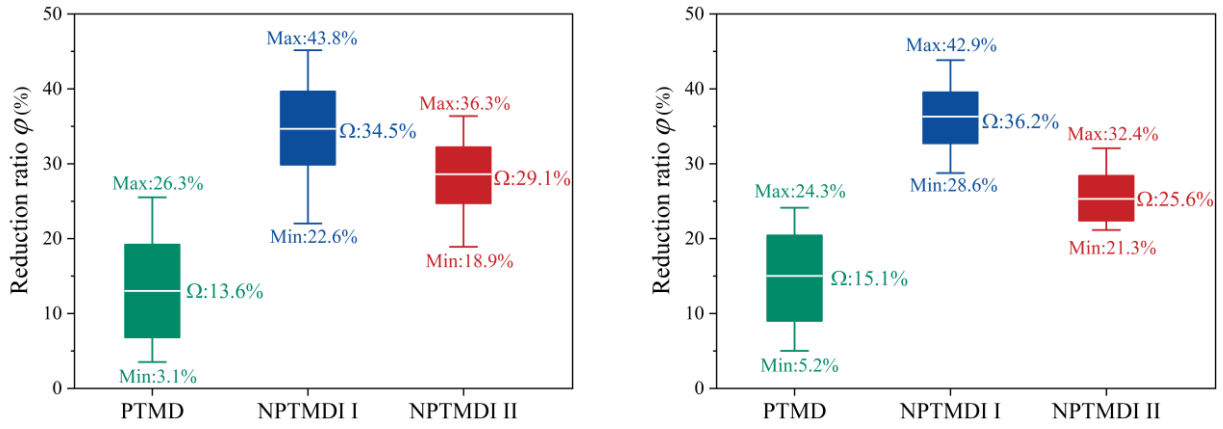

(a) (b)

Fig. 18. Top-floor response reduction ratios of different systems under perturbations of ξ_2. (a) Reduction ratios of peak displacement; (b) Reduction ratios of peak acceleration

6. Conclusions

In this study, two novel NPTMDIs are proposed for the vibration control of high-rise buildings subjected to wind loads. Their configurations and working mechanisms are introduced, and the analytical models of a benchmark building structure equipped with NPTMDIs are presented. Besides, the optimal parameters of the two NPTMDIs are attained based on the genetic algorithm. Moreover, the vibration control effectiveness and robustness of the proposed NPTMDIs are investigated and

compared with that of the conventional PTMD. Based on the analytical results, it can be concluded as follows:

(1) The developed NPTMDIs outperform the conventional PTMD with the same mass ratio in mitigating wind-induced responses. Compared to the uncontrolled scenario, the peak top-floor acceleration of the high-rise building is reduced by 24.12% with PTMD, 44.81% with NPTMDI I, and 34.28% with NPTMDI II.

(2) Compared to the conventional PTMD, the inerter in NPTMDI I and II effectively suppresses the tip mass oscillation, thereby reducing the risk of collision with the primary structure.

(3) The vibration control effectiveness of NPTMDIs depends on the installation location of inerter, and lower connection floors generally lead to more significant control effectiveness.

(4) The proposed NPTMDIs are more robust against the uncertainties of both structure and device parameters as compared to the conventional PTMD.

This study investigates the control effectiveness of NPTMDIs using linear single-degree-of-freedom (SDOF) and multiple-degree-of-freedom (MDOF) systems. Future research will employ nonlinear MDOF systems for a more comprehensive analysis and conduct experimental studies to validate the control performance of NPTMDIs.

Acknowledgment

The authors gratefully acknowledge the funding from the National Natural Science Foundation of China (No. 52208452), and Open Fund from State Key Laboratory of Coastal and Offshore Engineering (No. LP2315).

References

[1] Kwok K C S, Hitchcock P A, Burton M D. Perception of vibration and occupant comfort in wind-excited tall buildings. J Wind Eng Ind Aerodyn, 2009, 97(7-8): 368-380.

[2] Fu J, Zheng Q, Huang Y, et al. Design optimization on high-rise buildings considering occupant comfort reliability and joint distribution of wind speed and direction. Eng Struct, 2018, 156: 460-471.

[3] Jafari, M., Alipour A. Methodologies to mitigate wind-induced vibration of tall buildings: A state-of-the-art review. J Build Eng, 2021, 33: 101582.

[4] Saaed T E, Nikolakopoulos G, Jonasson J E, et al. A state-of-the-art review of structural control systems. J. Vib. Control, 2015, 21(5): 919-937.

[5] Setareh M, Ritchey J K, Baxter A J, et al. Pendulum tuned mass dampers for floor vibration control. J Perform Constr Fac, 2006, 20(1): 64-73.

[6] Roffel A J, Narasimhan S, Haskett T. Performance of pendulum tuned mass dampers in reducing the responses of flexible structures. J Struct Eng., 2013, 139(12): 04013019.
[7] Sacks MP, Swallow JC. Tuned mass dampers for towers and buildings. Structural Engineering in Natural Hazards Mitigation, 1993: 640-645.
[8] Tuan A Y, Shang G Q. Vibration control in a 101-floor building using a tuned mass damper. J Eng Appl Sci, 2014, 17(2): 141-156.
[9] Lu X, Chen J. Parameter optimization and structural design of tuned mass damper for Shanghai centre tower. Struct Des Tall Special Build, 2011, 20(4): 453-471.
[10] Lu X, Chen J. Mitigation of wind-induced response of Shanghai Center Tower by tuned mass damper. Struct Des Tall Special Build, 2011, 20(4): 435-452.
[11] Matta E. Modeling and design of bidirectional pendulum tuned mass dampers using axial or tangential homogeneous friction damping. Mech Syst Signal Process, 2019, 116: 392-414.
[12] Wang L, Nagarajaiah S, Shi W, et al. Study on adaptive-passive eddy current pendulum tuned mass damper for wind-induced vibration control. Struct Des Tall Special Build, 2020, 29(15): e1793.
[13] Wang L, Shi W, Li X, et al. An adaptive-passive retuning device for a pendulum tuned mass damper considering mass uncertainty and optimum frequency. Struct. control health monit, 2019, 26(7): e2377.
[14] Wang L, Shi W, Zhou Y. Adaptive-passive tuned mass damper for structural aseismic protection including soil–structure interaction. Soil Dyn. Earthquake Eng, 2022, 158: 107298.
[15] Miguel L F F, Lopez R H, Torii A J, et al. Reliability-based optimization of multiple folded pendulum TMDs through efficient global optimization. Eng Struct, 2022, 266: 114524.
[16] De Angelis M, Perno S, Reggio. A Dynamic response and optimal design of structures with large mass ratio TMD. Earthq Eng Struct D, 2012, 41(1): 41-60.
[17] Wang L, Zhou Y, Shi W. Seismic response control of a nonlinear tall building under mainshock–aftershock sequences using semi-active tuned mass damper. Int J Struct Stab Dy, 2023, 23(16n18): 2340027.
[18] Smith M C. Synthesis of mechanical networks: the inerter. IEEE Trans Automat Contr, 2002, 47(10): 1648-1662.
[19] Ma R, Bi K, Hao H. Inerter-based structural vibration control: A state-of-the-art review. Eng Struct, 2021, 243: 112655.
[20] Song J, Bi K, Ma R, et al. Vibration control of adjacent structures equipped with inerter-based dampers considering nonlinearities: Analytical and experimental studies. Mech Syst Signal Process, 2024, 206: 110903.
[21] Marian L, Giaralis A. Optimal design of a novel tuned mass-damper–inerter (TMDI) passive vibration control configuration for stochastically support-excited structural systems. Probablist Eng Mech, 2014, 38: 156-164.
[22] He W, Zhou Y, Wang Z, et al. Soil-dependent stochastic optimization of base isolation system with negative stiffness inerter damper subjected to non-stationary seismic excitation. Structures, 2024, 67: 106955.
[23] Ikago K, Saito K, Inoue N. Seismic control of single-degree-of-freedom structure using tuned viscous mass damper. Earthq Eng Struct D, 2012, 41(3): 453-474.
[24] Zhang J, Liu Y, Xue S. Analysis and experimental evaluation of an inertial eddy current damper for vibration control. Structures, 2024, 68: 107052.
[25] Lazar I F, Neild S A, Wagg D J. Using an inerter-based device for structural vibration suppression. Earthq Eng Struct D, 2014, 43(8): 1129-1147.
[26] Makris N, Kampas G. Seismic protection of structures with supplemental rotational inertia. J. Eng. Mech,

2016, 142(11): 04016089.
[27] Jangid R S. Seismic performance of a clutched inerter for structures with curved surface sliders. Structures, 2023, 49: 44-57.
[28] Ma R, Bi K, Hao H. A novel rotational inertia damper for amplifying fluid resistance: Experiment and mechanical model. Mech Syst Signal Process, 2021, 149: 107313.
[29] Zhang R, Zhao Z, Dai K. Seismic response mitigation of a wind turbine tower using a tuned parallel inerter mass system. Eng Struct, 2019, 180: 29-39.
[30] Giaralis A, Petrini F. Wind-induced vibration mitigation in tall buildings using the tuned mass-damper-inerter. J Struct Eng, 2017, 143(9): 04017127.
[31] Giaralis A, Petrini F. Optimum design of the tuned mass-damper-inerter for serviceability limit state performance in wind-excited tall buildings. Procedia Eng, 2017, 199: 1773-1778.
[32] Wang Q, Tian H, Qiao H, et al. Wind-induced vibration control and parametric optimization of connected high-rise buildings with tuned liquid-column-damper–inerter. Eng Struct, 2021, 226: 111352.
[33] Zhu Z, Lei W, Wang Q, et al. Study on wind-induced vibration control of linked high-rise buildings by using TMDI. J Wind Eng Ind Aerodyn, 2020, 205: 104306.
[34] Lu Z, Zhou C, Rong K, et al. Vibration reduction mechanism of a novel enhanced particle inerter device. Int J Struct Stab Dy, 2023, 23(01): 2350009.
[35] Khorsand S, Rofooei F R. H∞ optimum design and nonlinear seismic performance assessment of tuned-mass-damper-inerter (TMDI) supported by an auxiliary structure. Structures, 2024, 69: 107257.
[36] Li, Y, Li S, and Tan P. A novel tuned mass damper inerter: optimal design, effectiveness comparison, and robustness investigation. Structures, 2023, 55: 1262-1276.
[37] Su N, Peng S, Hong N, et al. Wind-induced vibration absorption using inerter-based double tuned mass dampers on slender structures. J. Build Eng, 2022, 58: 104993.
[38] Elias S. Vibration improvement of offshore wind turbines under multiple hazards. Structures, 2024, 59: 105800.
[39] Elias S, Beer M. Vibration control and energy harvesting of offshore wind turbines installed with TMDI under dynamical loading. Eng Struct, 2024, 315: 118459.
[40] Dai J, Xu Z D, Gai P P, et al. Optimal design of tuned mass damper inerter with a Maxwell element for mitigating the vortex-induced vibration in bridges. Mech Syst Signal Process, 2021, 148: 107180.
[41] Xu K, Dai Q, Bi K, et al. Closed-form design formulas of TMDI for suppressing vortex-induced vibration of bridge structures. Struct. control health monit, 2022, 29(10): e3016.
[42] Li Z, Ma R, Xu K, et al. Closed-form solutions for the optimal design of lever-arm tuned mass damper inerter (LTMDI). Mech Syst Signal Process, 2024, 206: 110889.
[43] Suthar S J, Banerji P. Inerter-assisted pendulum-tuned mass damper for across-wind response control of tall buildings. Eng Struct, 2023, 291: 116489.
[44] Li C, Pan H, Cao L. Pendulum-type tuned tandem mass dampers-inerters for crosswind response control of super-tall buildings. J Wind Eng Ind Aerodyn, 2024, 247: 105706.
[45] Wang M, Sun F. Displacement reduction effect and simplified evaluation method for SDOF systems using a clutching inerter damper. Earthq Eng Struct Dyn, 2018, 47(7): 1651-1672.
[46] Málaga-Chuquitaype C, Menendez-Vicente C, Thiers-Moggia R. Experimental and numerical assessment of the seismic response of steel structures with clutched inerters. Soil Dyn. Earthquake Eng, 2019, 121: 200-211.

[47] Li L, Liang Q. Seismic assessment and optimal design for structures with clutching inerter dampers. J. Eng. Mech, 2020, 146(4): 04020016.
[48] Liang Q, Li L. Optimal design for a novel inerter-based clutching tuned mass damper system. J. Vib. Control, 2020, 26(21-22): 2050-2059.
[49] Wang J, Zheng Y. Experimental validation, analytical investigation, and design method of tuned mass damper-clutching inerter for robust control of structures. Earthq Eng Struct D, 2023, 52(2): 500-523.
[50] Wu J C, Yang J N, Schmitendorf W E. Reduced-order H∞ and LQR control for wind-excited tall buildings. Eng Struct, 1998, 20(3): 222-236.
[51] Xu K, Hua X, Lacarbonara W, et al. Exploration of the nonlinear effect of pendulum tuned mass dampers on vibration control. J. Eng. Mech, 2021, 147(8): 04021047.
[52] Kaimal J C, Wyngaard J C J, Izumi Y, et al. Spectral characteristics of surface-layer turbulence. Q J Roy Meteor Soc, 1972, 98(417): 563-589.
[53] Murtagh P J, Basu B, Broderick B M. Along-wind response of a wind turbine tower with blade coupling subjected to rotationally sampled wind loading. Eng Struct, 2005, 27(8): 1209-1219.
[54] Pietrosanti D, De Angelis M, Basili M. A generalized 2-DOF model for optimal design of MDOF structures controlled by Tuned Mass Damper Inerter (TMDI). Int. J. Mech. Sci, 2020, 185: 105849.
[55] De Angelis M, Basili M, Pietrosanti D. On the optimal design and placement of Tuned-Mass-Damper-Inerter for Multi-Degree-Of-Freedom structures. Structures, 2023, 56: 104781.
[56] Soltani P, Deraemaeker. A Pendulum tuned mass dampers and tuned mass dampers: Analogy and optimum parameters for various combinations of response and excitation parameters. J. Vib. Control, 2022, 28(15-16): 2004-2019.